Poly(3-hexylthiophene) nanofiber networks for enhancing the morphology stability of polymer solar cells

CrossMark

Ligui Li, Daniel L. Jacobs, Yanke Che, Helin Huang, Benjamin R. Bunes, Xiaomei Yang, Ling Zang *

Department of Materials Science and Engineering, University of Utah, Salt Lake City, UT 84108, United States

ARTICLE INFO

ABSTRACT

A stable morphology in the photoactive layer is a prerequisite for increasing the lifetime of organic solar cells. Intense research efforts focusing on this research topic have typically resorted to complicated synthetic methods to reach this goal. Herein, the authors present a facile approach to directly achieve efficient polymer solar cells with a remarkably enhanced thermally stable morphology by constructing densely distributed poly(3-hexyl-thiophene) (P3HT) nanofibers in the pristine composite films with PCBM ([6,6]-phenyl-C61-butyric acid methyl ester) from solution without any post treatments. Controlled experiments reveal that the presence of numerous preformed P3HT nanofibers in the pristine films, with much larger size than P3HT and PCBM molecules, provides a fixed and rigid network to spatially confine the diffusion of PCBM molecules during thermal annealing, thus preventing the formation of large-scale PCBM crystals. This simple method represents a "one-step" way to prepare high performance photovoltaic devices with thermally stable morphologies and no necessary post treatments.

1. Introduction

Organic solar cells are promising candidates for the third-generation photovoltaic devices due to their low cost, solution processing, light weight and mechanical flexibility compared to their inorganic counterparts. The introduction of the bulk-heterojunction (BHJ) concept [1,2] dramatically increased the interfacial area between electronic donor (D) and acceptor (A) materials for highly efficient dissociation of excitons into free charges compared to a typical bilayer device [3], opening a new era for organic photovoltaic (OPV) devices. However, such a BHJ morphology can also create discontinuous pathways for separated electrons and holes and increase the probability of geminate recombination prior to charge extraction. Thus, the components morphology in photoactive layer must be optimized to have D–A interfaces within the exciton diffu-

sion length (∼10 nm) [4–6] while maintaining continuous phase separated D and A pathways for fast charge carrier transport to the corresponding electrodes [7,8]. This has been one of the major focuses in OPV research efforts and recently a power conversion efficiency (PCE) of ca. 9.0% was achieved using this BHJ architecture [9,10], pushing the technology closer to becoming a viable source of clean energy.

Spin coating is the commonly adopted fabrication method for BHJ organic solar cells as it allows for fast deposition over a large area at ambient conditions. However, fast solvent evaporation during the spin coating process can severely suppress the phase separation of the D–A components and greatly reduce the formation of continuous pathways for free charge carriers to the electrodes. Post treatments, such as thermal annealing [11–13], are commonly used to improve the morphology of photoactive layers. However, this annealing process requires sophisticated control over the annealing conditions, such as annealing temperature and time, otherwise uncontrolled

---

* Corresponding author.
  E-mail address: lzang@eng.utah.edu (L. Zang).

growth of large-scale PCBM crystals can occur and severely decrease device performance. Even under temperatures as low as 60 °C, well within the working temperatures of outdoor PV devices in summer, the diffusion of PCBM molecules to form large aggregates is still possible [14]. This gradual change of microstructures reduces the D–A interfacial area and eventually results in performance degradation of the devices.

Recently, several strategies have been developed to control the phase separation and enhance the thermal stability of polymer solar cells. For example, by introducing compatibilizers [15–17], cross-linkers [18–20] or using block copolymers [21–24], modifying the conjugated polymers backbones with controlled amount of disorder [25,26], or even using amorphous fullerene electronic acceptors [7,27,28], the morphology stability of conjugated polymer:fullerene BHJ-based solar cells were substantially improved. However, all aforementioned methods involve a chemistry process, which usually needs complicated molecular design and time-consuming, multiple-step synthesis followed by tedious purification steps. In addition, post treatments are still needed to increase the device performance. These requirements will complicate the device fabrication process and increase the production cost. Therefore, it still remains highly desirable (though challenging) to develop a facile method which can directly achieve high performances as well as highly stable morphologies for polymer photovoltaic devices without any chemical modification to the commercially available materials.

Previously, Yang et al. [29] confirmed that spatial confinement on both sides of the photoactive layers exerted by substrate and the thermally evaporated metal cap can strongly reduce the diffusion rate of PCBM molecules and thus the scale of PCBM domains in the composite films during thermal annealing. Inspired by this pioneering work, we further exert spatial confinement on PCBM crystallization in the photoactive layers by using a nano-scaffold of preformed P3HT nanofibers with length scales up to several microns. We find that after introduction of the additionally spatial confinement from numerous P3HT nanofibers, the diffusion of PCBM in the composite films is remarkably reduced and the thermal stability of corresponding polymer solar cells is also dramatically increased, resulting in a high performance polymer solar cell with substantially enhanced thermal stability. Our findings not only provide a novel and facile method to directly achieve high performance polymer solar cells with high thermal stability through a "one-step" process, but also indicate that spatial confinement is an effective way to manipulate the morphology for optoelectronic devices that show morphology dependent performance.

2. Methods section

2.1. Materials

Regiorandom P3HT (RRa-P3HT) and regioregular P3HT (RR-P3HT) with M_n of ~20 kDa (PDI: 2.0) and regioregularity better than 95% were purchased from Rieke Metals Inc.

Solvents such as anhydrous chlorobenzene (CB), *o*-dichlorobenzene (ODCB), tetralin (Tet), xylene (Xyl) and chloroform (CF) with HPLC grade were purchased from Sigma–Aldrich Co. Ltd. PCBM with purity higher than 99.5% was purchased from Nano C, Inc.

2.2. Sample preparations

Blend solutions of P3HT(RR and RRa):PCBM (1:1, w/w) were prepared by mixing P3HT and PCBM in 10 mL glass bottles. Solutions in CF, CB and ODCB were made with a P3HT concentration of 10 mg/mL by stirring the above mixtures overnight at 45 °C. RR-P3HT:PCBM solutions in Tet:Xyl (1:1, v/v) were prepared with a concentration of 7 mg/mL by stirring at 60 °C for 2 h and then left under slow stirring (ca. 100 rpm) at room temperature for 5 days to facilitate the growth of RR-P3HT nanofibers.

Thin films for XRD and UV–vis absorption spectrum measurements were prepared by direct spin coating of the solutions or dispersions onto pre-cleaned glass slides. Thin films for atomic force microscopy (AFM) and optical microscopy characterization were obtained by spin coating the solutions or dispersions onto glass substrates with a pre-deposited, ca. 50 nm, poly(ethylenedioxythiophene):poly(styrene sulfonate) (PEDOT:PSS) layer on the surface. Thermal annealing was performed in a vacuum oven filled with ultra high purity argon.

Solar cells were fabricated under ambient conditions according to device fabrication procedures reported elsewhere [30]. First, a 50 nm PEDOT:PSS layer was spun onto a pre-cleaned glass substrate covered with 120 nm pre-patterned indium tin oxide (ITO) conductive layer (with sheet resistance of 5–15 Ω/□). Second, the photoactive layer was deposited via spin coating the prepared solution to a thickness of ca. 100–120 nm. Finally, the devices were completed with cathode deposition by sequential evaporation of a 1 nm LiF layer and 100 nm Al.

Space-charge limited current (SCLC) was used to calculate the mobility of P3HT:PCBM composite films prepared from different solvents. The devices for the mobility measurements were fabricated in an identical manner, except that a layer of 100 nm gold was thermally evaporated on P3HT:PCBM thin film instead of the LiF/Al layer to produce hole-only devices. The detailed calculation method of SCLC mobility can be found in Supporting information.

2.3. Characterizations

AFM measurements were conducted on a Veeco MultiModeV SPM instrument in intermittent contact (tapping) mode. Images were acquired with 512×512 points and scanning rate of ~0.5 Hz per line. UV–vis absorption spectra were acquired on a Perkin-Elmer Lambda 2 spectrophotometer. Wide angle X-ray diffraction (WAXD) profiles were obtained by using a Bruker D8 Discover Reflector with an X-ray generation power of 40 kV tube voltage and 40 mA tube current. The diffraction was recorded at a θ–2θ symmetry scanning mode with scan angles from 3.5° to 13°. Transmission electron microscopy (TEM) images were acquired on a JEOL 2010 TEM.

Solar cell performances were characterized with a Keithley-236 source measure unit at room temperature. The cells were illuminated by a Newport 150W Xenon lamp (filtered by an AM1.5G filter) at an intensity of 100 mW cm^{-2}.

3. Results and discussion

P3HT is known to crystallize into ribbon-like nanofibers in poor solvents or solvent mixtures [31–33]. Initially, P3HT:PCBM films with high P3HT crystallinity were prepared by using Tet:Xyl (1:1, v/v) mixture in which Tet shows poor solubility for RR-P3HT but a high solubility for PCBM [34–37]. In addition, this solvent mixture can ensure the formation of homogenous and pinhole-free films for devices (Fig. S2). Fig. 1b displays the UV–vis absorption spectra of RR-P3HT in various solvents including CF, ODCB, Xyl and Tet after storing in room temperature for 5 days. Of the four solutions, Xyl and Tet show obvious vibronic absorption peaks centered at 600 nm even with the lower concentration of 1 mg/mL. The absorption at ca. 600 nm is proven to correlate with the interchain π–π stacking of P3HT [38–40]. Therefore, the appearance of this absorption peak implies that RR-P3HT can indeed form crystalline aggregates in Xyl and Tet. On the contrary, solutions of 10 mg/mL RR-P3HT in CF and ODCB do not show absorption peaks at 600 nm, indicating P3HT remains molecularly dissolved in these two solutions. As for the pristine RR-P3HT:PCBM films prepared from the above solvents, WAXD measurements were conducted to preliminarily check the P3HT crystallinity in the composite films. As shown in Fig. 1c, all the pristine RR-P3HT:PCBM composite films show two resolved diffraction peaks centered at ca. $2\theta = 5.4°$ and $10.6°$, which are assigned to the reflection of crystallographic (1 0 0) and (2 0 0) plane of crystalline P3HT, respectively. As expected, the film prepared from Tet:Xyl solvent mixture aged for 5 days at room temperature shows much higher P3HT crystallinity than those prepared from CF and ODCB, evidenced by its stronger diffraction intensity. As a control, RR-P3HT:PCBM films with low P3HT crystallinity were made from the Tet:Xyl solution by heating the solution to 70 °C and spin coating on a hot glass substrate also maintained at 70 °C. The film (indicated as Tet:Xyl@70 °C) shows very low (1 0 0) diffraction intensity that is comparable to that in film prepared from CF. Crystalline grain sizes were calculated from the WAXD results using the Scherrer equation. RR-P3HT:PCBM films prepared from Tet:Xyl show a crystalline domain size of 13.1 nm, which is much larger than that of 7.8 nm, 9.8 nm and 8.0 nm obtained in CF, ODCB, and Tet:-Xyl@70 °C samples, respectively. SCLC hole mobility measurements (Fig. 1d) also show a similar trend to the WAXD results, implying that the very high P3HT crystallinity in the composite film prepared from Tet:Xyl solvent mixture can help to improve the hole carrier transport and probably enhance the performance of photovoltaic devices.

To investigate the morphology of RR-P3HT:PCBM composite films prepared from different solvents, AFM characterization was used. As shown in Fig. 2a, the surface of the
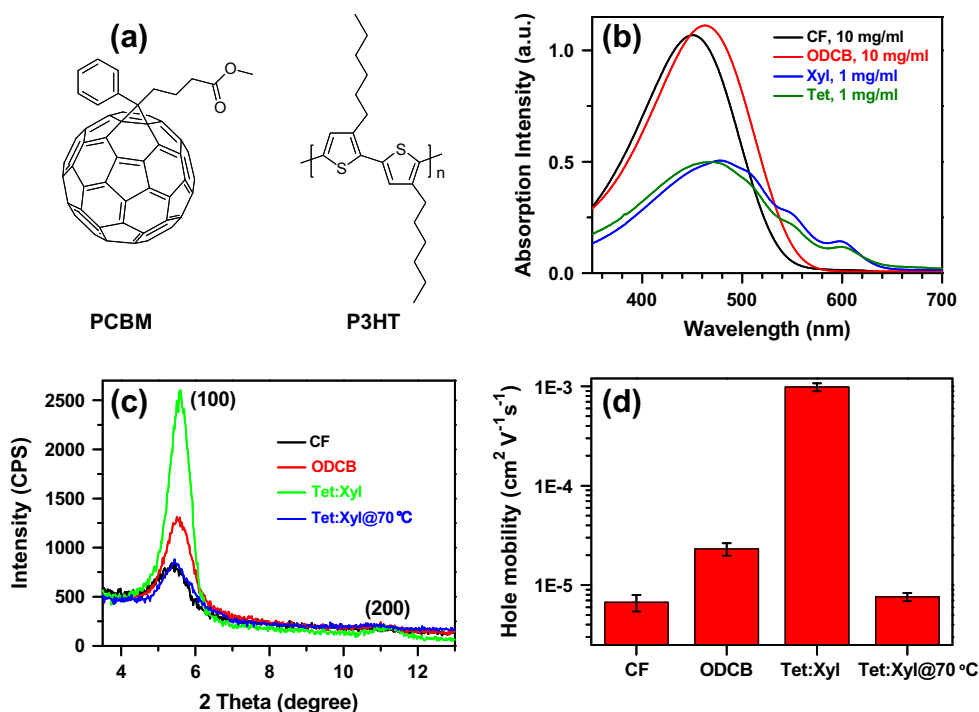
Fig. 1. (a) Molecular structures of PCBM and RR-P3HT; (b) UV–vis absorption spectra of RR-P3HT in CF, ODCB, Xyl and Tet after storing at room temperature for 5 days; (c) X-ray diffraction profiles (normalized to 100 nm) and (d) SCLC hole mobility of RR-P3HT:PCBM (1:1, w/w) composite films prepared from room temperature CF, ODCB, Tet:Xyl (1:1, v/v) and Tet:Xyl (1:1, v/v) at 70 °C.
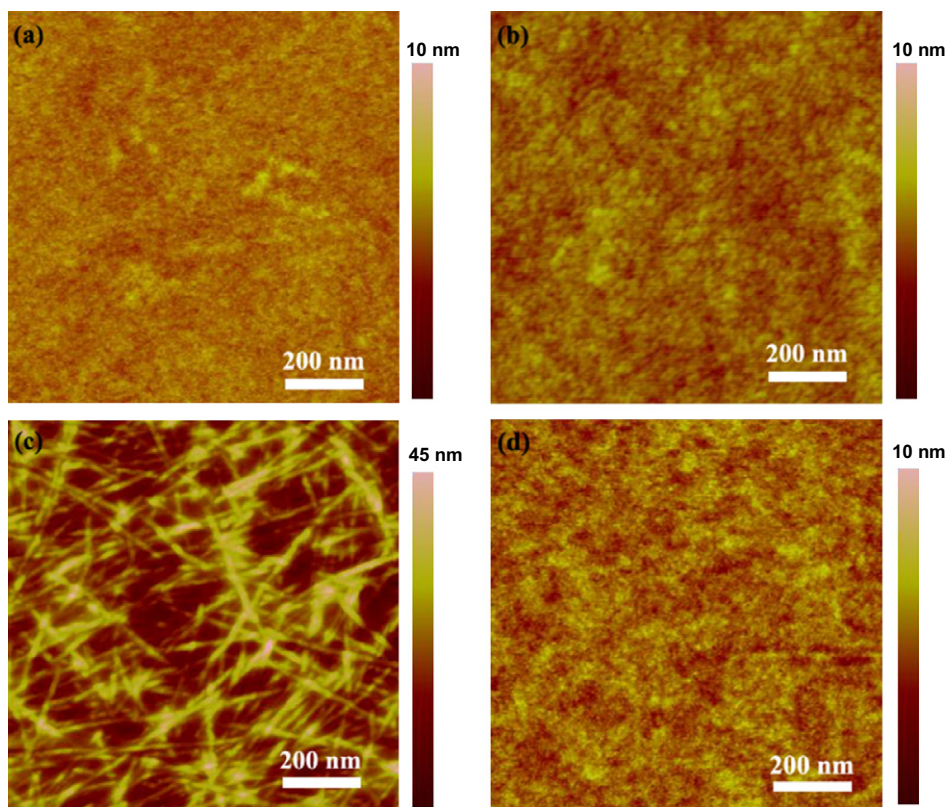
Fig. 2. AFM topography images showing the morphology of RR-P3HT:PCBM (1:1, w/w) pristine films spin-coated from different solvents. (a) CF; (b) ODCB; (c) Tet:Xyl and (d) Tet:Xyl@70 °C.

film prepared from CF is very smooth and contains no discernable P3HT fibers. For the RR-P3HT:PCBM film prepared from low volatile ODCB, some seemingly short P3HT nanofibers can be observed (Fig. 2b). Whereas, in the film prepared from Tet:Xyl solvent mixture (Fig. 2c), homogenous P3HT nanofibers with lengths up to several microns and straight appearance are observed throughout the film. In addition, no PCBM large crystals (with micrometer scale) are observed, which indicates that the P3HT nanofiber network is imbedded in the matrix of PCBM nanodomains [41]. In contrast, the film spin-coated from Tet:Xyl@70 °C only shows a very smooth surface and no obvious P3HT fibers are observed (Fig. 2d).

In an attempt to study the morphology stability of pristine composite films with varying degrees of P3HT crystallinity described above, all the films were subjected to thermal annealing at 150 °C for 15 h. For comparison, thermal annealing on control film prepared from Tet:Xyl@70 °C along with the film composed of RRa-P3HT was also conducted under the same condition. The results are shown in Fig. 3. After thermal annealing, films from CF, CB and ODCB solvents (Fig. 3a, b and c respectively), which show little to moderate degrees of P3HT crystallinity, demonstrate a high density of PCBM crystals all with similar sizes of ca. 10 μm. For the films prepared from the Tet:Xyl solvent (Fig. 3d), which have the highest P3HT crystallinity from all the films investigated, nanoscale phase separation with PCBM is maintained and very few micron sized crys-

tals are visible (Fig. S3). Conversely, films prepared from the hot Tet:Xyl solvent mixture resulted in high density of PCBM crystals with sizes (lengths) ranging from a few microns to ca. 100 μm (Fig. 3e), which is in sharp contrast to that observed in Fig. 3d. As a reference, the film composed of PCBM and RRa-P3HT (no crystalline P3HT phase) shows only a few but much larger and longer PCBM crystals (Fig. 3f). Based on these observations, we can conclude that the thermal morphology stability (*TMS*) of the four composite films prepared from different solutions follows the order: $TMS_{Tet:Xyl} \gg TMS_{ODCB} \approx TMS_{CB} > TMS_{CF}$.

The above TMS order of RR-P3HT:PCBM films prepared from different solutions matches that of P3HT crystallinity in pristine films indicated in Figs. 1c and 2. This suggests that higher P3HT crystallinity in solution results in greater thermal morphology stability. Additionally, the tremendous thermal stability difference observed in films prepared from Tet:Xyl and Tet:Xyl@70 °C further confirms that the crystallinity of P3HT in pristine films strongly influences the thermal stability. From these results, we speculate that the P3HT nanofibers in pristine films can limit the diffusion of PCBM molecules and suppress the growth of large PCBM crystals during thermal annealing and thus result in more stable morphologies.

To get a deeper insight into the origin of the highly stable morphology of RR-P3HT:PCBM composite films prepared from Tet:Xyl, we use UV–vis absorption spectrum to study the structural changes of P3HT phase after long
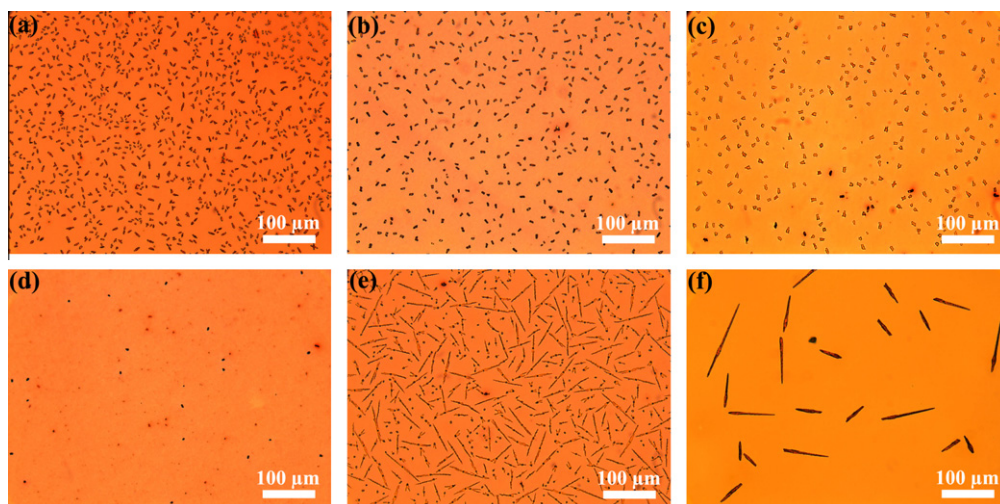
Fig. 3. Optical microscopy images showing the morphology of (a–e) RR-P3HT:PCBM (1:1, w/w) and (f) RRa-P3HT:PCBM (1:1, w/w) composite films prepared from different solvents after thermal annealing at 150 °C for 15 h. (a) CF; (b) CB; (c and f) ODCB; (d) Tet:Xyl; and (e) Tet:Xyl@70 °C.
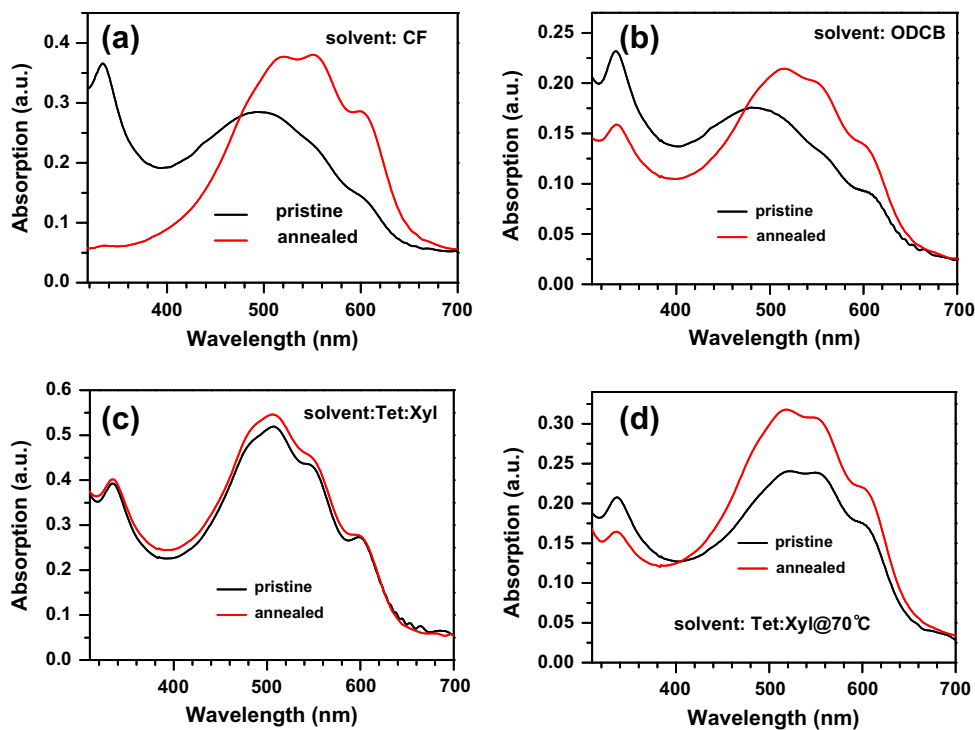
Fig. 4. UV–vis absorption spectra of pristine and annealed (150 °C for 15 h) RR-P3HT:PCBM films prepared from (a) CF; (b) ODCB; (c) Tet:Xyl and (d) Tet:Xyl@70 °C.

time thermal annealing. As shown in Fig. 4, all the composite films prepared from CF, CB, ODCB and Tet:Xyl@70 °C show remarkable increase of crystalline order, as evidenced by a significant increase of absorption intensity in the long wavelength region. This observation indicates that within these films P3HT crystallization is greatly suppressed due to the fast solvent evaporation during spin coating. In contrast, for the film prepared from Tet:Xyl

mixture P3HT has already crystallized into nanofibers in solution and is thus not affected by subsequent spin coating or thermal annealing process. In addition, the absorption peak centered at ca. 335 nm is assigned to the absorption of PCBM in solid film. It is expected when PCBM in composite films diffuses to form large crystalline domains, its absorption intensity will substantially decrease. After long time thermal annealing, of the four samples

shown in Fig. 4 only the composite film prepared from Tet:Xyl solvent mixture shows the same absorption intensity as that in pristine film, implying that indeed only PCBM in the composite film prepared from Tet:Xyl remains in nanoscale domains, while in other three films PCBM molecules diffuse to form large aggregates. This observation is consistent with that observed in Fig. 3. We can further conclude here that excessive PCBM diffusion during thermal annealing is blocked in the film prepared from Tet:Xyl.

Taking all the above results into account, we can conclude here that the thermally stable morphology of Fig. 3d is unambiguously correlated with the preformed network of numerous P3HT crystalline nanofibers. It is known that when cooled down to room temperature, the dissolved P3HT molecules in poor solvent will undergo coil-to-rod conformation change and crystallize into long P3HT nanofiber through intermolecular π–π stacking [33,42,43]. When spin-coating from the Tet:Xyl dispersion, the preformed P3HT fibers will create a network with nanoscale domains of PCBM filling in the meshes. During thermal annealing process, since the crystalline P3HT nanofibers have much higher rigidity than P3HT single molecular chains, the movement of P3HT nanofibers is negligible as compared to the crystallizable P3HT molecular chains frozen in the amorphous domains. Additionally, the size of crystalline P3HT nanofiber is much larger than both the single P3HT molecular chain and PCBM molecule in all three dimensions (see Table 1). Therefore, the fixed and rigid network composed of P3HT nanofibers will substantially hinder the free diffusion of PCBM molecules and only allow the PCBM molecules in individual mesh to crystallize/fuse together (see the right column in Fig. 5). This is actually the introduction of spatial confinement in the film. Consequently, this confinement contributes to a composite film with very high P3HT crystallinity as well as homogenous PCBM nanocrystals, even after longtime thermal annealing. On the contrary, in the pristine films prepared by spin coating from solvents in which P3HT shows very good solubility, P3HT exists predominantly as amorphous domains due to the fast solvent evaporation during spin coating process. When post thermal annealing is adopted to improve the film morphology for efficient PV devices, both the amorphous P3HT and PCBM molecules will be activated to crystallize. Because there is no such fixed, rigid and large-scale network of

P3HT nanofibers in the film, the confinement of flexible P3HT chains on PCBM molecular diffusion is weak [44,45]. Therefore, PCBM molecules can freely diffuse to reach a more stable state of thermodynamic equilibrium, eventually forming large-scale PCBM crystals (left column in Fig. 5). It should be pointed out that though decreasing the regioregularity of conjugated polymers has been proven to be an effect way to enhance the thermal stability to some extent by lowering the driving force for polymer crystallization [25,26]. However, in our case we believe that it is the structural confinement of P3HT nanofibers on the diffusion of PCBM molecules that accounts for the enhanced thermal stability and not the regioregularity of P3HT. As shown in Fig. 3f, the density of large PCBM crystals is substantially decreased due to the noncrystallizable RRa-P3HT chains within the film, however the free diffusion of PCBM still exists in this film as evidenced by the less but much larger and longer PCBM crystals formed after longtime annealing. Furthermore, it is important to note that the stable morphology can only be realized when a solvent that has both low solubility for P3HT and high solubility of PCBM (see Fig. S4) is used. When a solvent or solvent mixture with low solubility of PCBM is used, numerous PCBM nuclei (in the form of submicron or larger clusters/aggregates) are already formed in pristine films after spin coating [14,46–49]. With the significant presence of PCBM nucleation centers, the crystallization of PCBM is much more efficient and can form large PCBM crystals even after short-time thermal annealing.

The most exciting expectation for the network of P3HT nanofibers is to prepare efficient and highly thermal stable OPV devices. As shown in Fig. 6a, except for comparable V_{oc} (open-circuit voltage) of ca. 0.6 V, the typical device prepared from Tet:Xyl solvent mixture shows an overall increase in performance with a *FF* (filling factor) of 0.52 and J_{sc} (short-circuit current density) of 10.82 mA/cm^2 compared to pristine devices prepared from CF and ODCB. Consequently, a PCE of 3.37% is readily achieved in this device while the pristine devices prepared from CF and ODCB only show a PCE of 0.51% and 0.98%, respectively. Therefore, high performance devices can be directly obtained from Tet:Xyl solvent mixture, mainly benefiting from the large number of continuous pathways for fast hole transport in the pristine films [13,32,33,50–52].

Fig. 6b demonstrates the thermal stability of devices prepared from different solvents. For the devices prepared

Table 1
Summary of the sizes of P3HT molecule chain, PCBM molecule and P3HT crystalline fibers in RR-P3HT:PCBM composite film prepared by using Tet:Xyl as solvent.

	Length (nm)	Width (nm)	Height (nm)
Fully extended P3HT molecule chain	48.2[a]	–	3.5[b]
PCBM molecule	~1.4[b]	~0.8[b]	~1.4[b]
P3HT crystalline fibers	>2000[c]	20–35[d]	13.1[e]

[a] The length is evaluated by $L \times n$, where L is the length of repeating unit in P3HT backbone derived from the ChemOffice software, n is the number of repeating unit of P3HT calculated from its molecular weight.
[b] Evaluated from ChemOffice software.
[c] Evaluated from the AFM image shown in Fig. 2c and Fig. S6.
[d] Measured from the SEM image (Fig. S7).
[e] Calculated from the FWH of crystallographic (1 0 0) plane in the WAXD profiles in Fig. 1a.

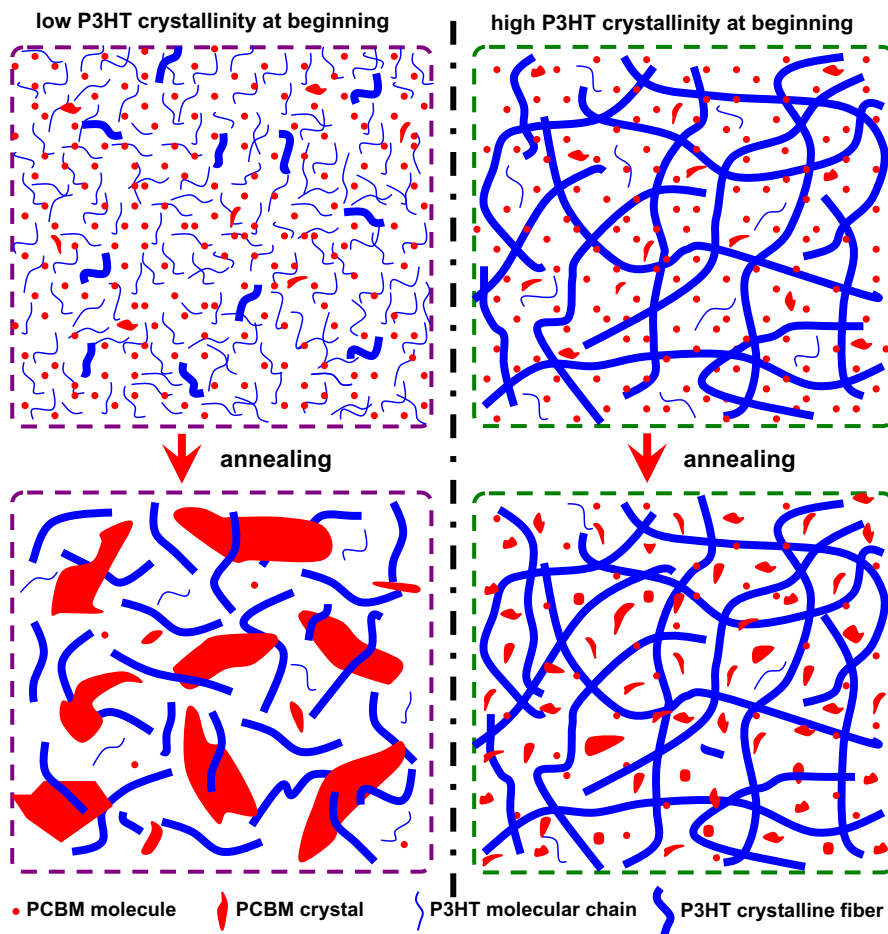**low P3HT crystallinity at beginning** | **high P3HT crystallinity at beginning**

Fig. 5. Sketch showing the morphology obtained after longtime thermal annealing with (right column) and without (left column) the spatial confinement effect of P3HT nanofibers in pristine films.
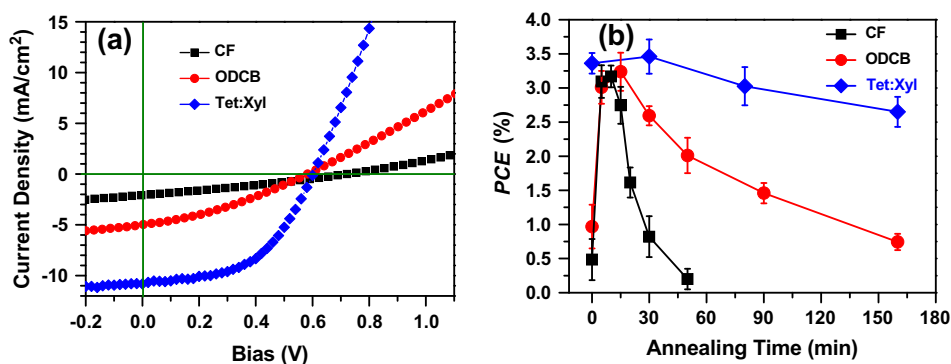

Fig. 6. (a) *J–V* curves of pristine solar cells prepared from different solvents; (b) the thermal stability of devices annealed at 150 °C for different time (each curve was based on the statistic of six devices).

from CF solvent, thermal annealing can remarkably increase the PCE to 3.22% in about 10 min. However, extended annealing time quickly degrades the device performance to that before thermal annealing within 40 min. As for the devices prepared from ODCB, a similar trend was also observed but the slightly increased P3HT

crystallinity resulted in slower performance degradation. As expected, the preformed network of P3HT nanofibers prepared from Tet:Xyl dramatically increases the thermal stability of PV devices. After thermal annealing at 150 °C for 160 min, the devices prepared from Tet:Xyl retained ca. 80% of the initial PCE. Therefore, the preformed network

of P3HT nanofibers can substantially enhance the thermal morphology stability of devices prepared from Tet:Xyl solvent mixture. The simple method presented here represents a new way to prepare efficient PV devices with highly thermally stable morphology through "one-step" process.

4. Conclusion

We are able to demonstrate that efficient polymer solar cells with a thermally stable morphology can be directly achieved by creating a network of densely distributed crystalline conjugated polymer nanofibers. The preformed conjugated polymer nanofibers network not only provides continuous pathways for hole carries transport but also exerts spatial confinement to prevent excessive diffusion of PCBM molecules, which contributes to a high performance device with substantially enhanced morphology stability. This simple method represents a new way to directly achieve efficient polymer solar cells with highly thermally stable morphology through a "one-step" process, which can be useful for lowering the production cost in large scale OPV devices.

Acknowledgments

Appendix A. Supplementary material

Supplementary data associated with this article can be found, in the online version, at http://dx.doi.org/10.1016/j.orgel.2013.02.032.

References

[1] G. Yu, J. Gao, J.C. Hummelen, F. Wudl, A.J. Heeger, Science 270 (1995) 1789.
[2] J.J.M. Halls, C.A. Walsh, N.C. Greenham, E.A. Marseglia, R.H. Friend, S.C. Moratti, A.B. Holmes, Nature 376 (1995) 498.
[3] C.W. Tang, Appl. Phys. Lett. 48 (1986) 183.
[4] S. Günes, H. Neugebauer, N.S. Sariciftci, Chem. Rev. 107 (2007) 1324.
[5] A. Huijser, B.M.J.M. Suijkerbuijk, R.J.M.K. Gebbink, T.J. Savenije, L.D.A. Siebbeles, J. Am. Chem. Soc. 130 (2008) 2485.
[6] A.W. Hains, Z. Liang, M.A. Woodhouse, B.A. Gregg, Chem. Rev. 110 (2010) 6689.
[7] C.-Y. Chang, C.-E. Wu, S.-Y. Chen, C. Cui, Y.-J. Cheng, C.-S. Hsu, Y.-L. Wang, Y. Li, Angew. Chem. Int. Ed. 50 (2011) 9386.
[8] J. Peet, J.Y. Kim, N.E. Coates, W.L. Ma, D. Moses, A.J. Heeger, G.C. Bazan, Nat. Mater. 6 (2007) 497.
[9] Z. He, C. Zhong, X. Huang, W.-Y. Wong, H. Wu, L. Chen, S. Su, Y. Cao, Adv. Mater. 23 (2011) 4636.
[10] Z. He, C. Zhong, S. Su, M. Xu, H. Wu, Y. Cao, Nat. Photon. 6 (2012) 591.
[11] X.N. Yang, J. Loos, S.C. Veenstra, W.J.H. Verhees, M.M. Wienk, J.M. Kroon, M.A.J. Michels, R.A.J. Janssen, Nano Lett. 5 (2005) 579.
[12] W. Ma, C. Yang, X. Gong, K. Lee, A. Heeger, Adv. Funct. Mater. 15 (2005) 1617.
[13] S.S. van Bavel, E. Sourty, G.d. With, J. Loos, Nano Lett. 9 (2009) 507.
[14] X.N. Yang, J.K.J. van Duren, R.A.J. Janssen, M.A.J. Michels, J. Loos, Macromolecules 37 (2004) 2151.
[15] Z. Zhou, X. Chen, S. Holdcroft, J. Am. Chem. Soc. 130 (2008) 11711.
[16] J.B. Kim, K. Allen, S.J. Oh, S. Lee, M.F. Toney, Y.S. Kim, C.R. Kagan, C. Nuckolls, Y.-L. Loo, Chem. Mater. 22 (2010) 5762.
[17] K. Sivula, Z.T. Ball, N. Watanabe, J.M.J. Fréchet, Adv. Mater. 18 (2006) 206.
[18] B.J. Kim, Y. Miyamoto, B. Ma, J.M.J. Fréchet, Adv. Funct. Mater. 19 (2009) 2273.
[19] B. Gholamkhass, S. Holdcroft, Chem. Mater. 22 (2010) 5371.
[20] H.J. Kim, A.-R. Han, C.-H. Cho, H. Kang, H.-H. Cho, M.Y. Lee, J.M.J. Fréchet, J.H. Oh, B.J. Kim, Chem. Mater. 24 (2012) 215.
[21] D.A. Kamkar, M. Wang, F. Wudl, T.-Q. Nguyen, ACS Nano 6 (2012) 1149.
[22] S. Miyanishi, Y. Zhang, K. Tajima, K. Hashimoto, Chem. Commun. 46 (2010) 6723.
[23] J.U. Lee, Y.D. Kim, J.W. Jo, J.P. Kim, W.H. Jo, J. Mater. Chem. 21 (2011) 17209.
[24] M. Heuken, H. Komber, T. Erdmann, V. Senkovskyy, A. Kiriy, B. Voit, Macromolecules 45 (2012) 4101.
[25] C.H. Woo, B.C. Thompson, B.J. Kim, M.F. Toney, J.M.J. Fréchet, J. Am. Chem. Soc. 130 (2008) 16324.
[26] K. Sivula, C.K. Luscombe, B.C. Thompson, J.M.J. Fréchet, J. Am. Chem. Soc. 128 (2006) 13988.
[27] X. Meng, W. Zhang, Z.a. Tan, Y. Li, Y. Ma, T. Wang, L. Jiang, C. Shu, C. Wang, Adv. Funct. Mater. 22 (2012) 2187.
[28] Y. Zhang, H.-L. Yip, O. Acton, S.K. Hau, F. Huang, A.K.-Y. Jen, Chem. Mater. 21 (2009) 2598.
[29] X.N. Yang, A. Alexeev, M.A.J. Michels, J. Loos, Macromolecules 38 (2005) 4289.
[30] M.M. Wienk, M. Turbiez, J. Gilot, R.A.J. Janssen, Adv. Mater. 20 (2008) 2556.
[31] K.J. Ihn, J. Moulton, P. Smith, J. Polym. Sci. Part B: Polym. Phys. 31 (1993) 735.
[32] S. Berson, R.D. Bettignies, S. Bailly, S. Guillerez, Adv. Funct. Mater. 17 (2007) 1377.
[33] L.G. Li, G.H. Lu, X.N. Yang, J. Mater. Chem. 18 (2008) 1984.
[34] L.G. Li, H.W. Tang, H.X. Wu, G.H. Lu, X.N. Yang, Org. Electron. 10 (2009) 1334.
[35] M. Schubert, D. Dolfen, J. Frisch, S. Roland, R. Steyrleuthner, B. Stiller, Z. Chen, U. Scherf, N. Koch, A. Facchetti, D. Neher, Adv. Energy Mater. 2 (2012) 369.
[36] The purpose we used the Tet:Xyl (1:1, v/v) mixture instead of Tet is to enhance the wetting of PEDOT:PSS in device preparation and avoid the formation of pinholes.
[37] C.N. Hoth, S.A. Choulis, P. Schilinsky, C.J. Brabec, J. Mater. Chem. 19 (2009) 5398.
[38] P.J. Brown, D.S. Thomas, A. Köhler, J.S. Wilson, J.-S. Kim, C.M. Ramsdale, H. Sirringhaus, R.H. Friend, Phys. Rev. B 67 (2003) 064203.
[39] M.C. Gurau, D.M. Delongchamp, B.M. Vogel, E.K. Lin, D.A. Fischer, S. Sambasivan, L.J. Richter, Langmuir 23 (2007) 834.
[40] T. Yamamoto, D. Komarudin, M. Arai, B.-L. Lee, H. Suganuma, N. Asakawa, Y. Inoue, K. Kubota, S. Sasaki, T. Fukuda, H. Matsuda, J. Am. Chem. Soc. 120 (1998) 2047.
[41] X.N. Yang, J.K.J. van Duren, M.T. Rispens, J.C. Hummelen, R.A.J. Janssen, M.A.J. Michels, J. Loos, Adv. Mater. 16 (2004) 802.
[42] S. Samitsu, T. Shimomura, S. Heike, T. Hashizume, K. Ito, Macromolecules 41 (2008) 8000.
[43] M. He, L. Zhao, J. Wang, W. Han, Y.L. Yang, F. Qiu, Z.Q. Lin, ACS Nano 4 (2010) 3241.
[44] B. Watts, W.J. Belcher, L. Thomsen, H. Ade, P.C. Dastoor, Macromolecules 42 (2009) 8392.
[45] W.-R. Wu, U.-S. Jeng, C.-J. Su, K.-H. Wei, M.-S. Su, M.-Y. Chiu, C.-Y. Chen, W.-B. Su, C.-H. Su, A.-C. Su, ACS Nano 5 (2011) 6233.
[46] H. Hoppe, N.S. Sariciftci, J. Mater. Chem. 16 (2006) 45.
[47] M.A. Ruderer, S. Guo, R. Meier, H.-Y. Chiang, V. Körstgens, J. Wiedersich, J. Perlich, S.V. Roth, P. Müller-Buschbaum, Adv. Funct. Mater. 21 (2011) 3382.
[48] S. Bertho, W.D. Oosterbaan, V. Vrindts, J. D'Haen, T.J. Cleij, L. Lutsen, J. Manca, D. Vanderzande, Org. Electron. 10 (2009) 1248.
[49] K.-S. Chen, H.-L. Yip, C.W. Schlenker, D.S. Ginger, A.K.-Y. Jen, Org. Electron. 13 (2012) 2870.
[50] H. Xin, F.S. Kim, S.A. Jenekhe, J. Am. Chem. Soc. 130 (2008) 5424.
[51] G. Ren, P.-T. Wu, S.A. Jenekhe, ACS Nano 5 (2011) 376.
[52] G. Li, V. Shrotriya, J. Huang, Y. Yao, T. Moriarty, K. Emery, Y. Yang, Nat. Mater. 4 (2005) 864.